

# Detection of internal delamination in multi-layer composites using wavelet packets combined with modal parameter analysis

Z. Wei, L.H. Yam<sup>\*</sup>, L. Cheng

*Department of Mechanical Engineering, The Hong Kong Polytechnic University, Hung Hom, Kowloon, Hong Kong*

## Abstract

This paper presents a study on active detection of delamination for multi-layer composites using a combination of modal analysis and wavelet transform. The analysis of modal parameters for multi-layer composites with internal delamination is carried out, and energy spectrum of wavelet packet decomposition of structural dynamic response is investigated. For several samples with different delamination dimensions and support conditions, the finite element method is used to study the relationship between delamination dimension and damage-induced change of structural physical property. Results show that delamination leads to a variation of energy dissipation in plate vibration, and it is mode-dependent. For relatively small delamination, the damage-induced changes of natural frequencies and mode shapes are too slight to be detected practically. However, by means of analysis on energy spectrum of wavelet packet decomposition even smaller delamination can be detected using the measured dynamic response signals.

© 2003 Elsevier Ltd. All rights reserved.

*Keywords:* Composite; Internal delamination; Wavelet packets; Modal analysis

## 1. Introduction

With the wide application of composites in aerospace industry, the nondestructive testing (NDT) of composite components is absolutely necessary for the enhancement and control of quality and the safe running of aerospace structures. Fiber-reinforced multi-layer composites are widely used in structures of aerospace, vehicles, architecture and light industrial products. Under aging, chemical corruption and mechanical impact, four main types of damage may be induced, i.e. delamination, matrix cracking, fiber breakage and interfacial debonding. Generally, failure is due to a combination of these damages. Early detection of initial damage can prevent a catastrophic failure or structural deterioration beyond repair. It is then critical to detect and distinguish these damages for practical materials or structures [1–5].

Due to the anisotropy and the complexity of internal structure, it is more complicated to carry out NDT for damage detection of composites than that of metals. The conventional NDT methods, such as C-scan, X-ray, AE, and eddy current, require expensive equipment and strict environmental condition. They are also impracti-

cal for application under in-service condition. Hence, vibration-based NDT has been developed for damage detection, especially for active damage detection, i.e., no external equipment is needed for generating excitation to the structure. Dynamic response, modal parameters, and spectrum analysis are applied in the field of material damage detection [6–21]. The basic idea in vibration-based damage detection is that these parameters depend on the physical properties of the structural to be inspected. Therefore, changes in physical properties of a structure due to damage can result in detectable variations in its parameters, such as natural frequencies, displacement or strain mode shapes and modal damping. The key problem is how to extract useful features from the vibration signals for damage detection or identification. Among many signal analysis methods, the FFT is one of the most widely used and well-established methods. As dangerous damage always results from the development or accumulation of very tiny damage, it is very important and meaningful to find the damage at its early stage of development. However, when the damage is very small, the damage-induced changes of physical properties in composites are always too insignificant to discover the damage using the FFT-based method. In addition, the measured vibration signals are often contaminated by noise. Therefore, the wavelet transform-based method for vibration signal analysis is gradually

<sup>\*</sup> Corresponding author. Tel.: +852-2766-7820; fax: +852-2365-4703.

*E-mail address:* [mmlhyam@polyu.edu.hk](mailto:mmlhyam@polyu.edu.hk) (L.H. Yam).

adopted in many fields due to its good time-frequency localization, but few publications can be found about its application to vibration-based damage detection of composites [22–24].

Despite of the extensive studies of vibration analysis on damaged laminated composites [25–31], the problem is still not fully understood and only few effective and practical techniques are found for early detection and size identification of damage such as internal delamination. This paper, therefore, focuses on the study of a practical method for effective detection of internal delamination in fibrous laminated plates by combining numerical analysis on structural modal parameters with wavelet packet decomposition of vibration signals.

## 2. Finite element model

Finite element method (FEM) is used to compute the modal parameters such as natural frequency, mode shape and modal strain of each mode for a laminated composite plate with or without delamination. In order to numerically analyze the vibration response of delaminated composite plates, it is important to have an effective FE model for accurately evaluating the effects of material anisotropy and delamination. As composite plates of moderate thickness are investigated in this paper, three-dimensional FE model is adopted to consider the effects of transverse shear stress on plate performance.

The finite element used for dynamic behavior analysis of a multi-layer composite plate is an eight-node rectangular thin plate as shown in Fig. 1. For each node, there are three degrees of freedom, i.e., translations along the global coordinate axes of  $x$ ,  $y$  and  $z$ , respectively. The element thickness is assigned to be equal to that of the corresponding individual lamina. The local element coordinate system  $(x_1, y_1, z_1)$  is arranged with the first axis being coincident with the fiber direction. All

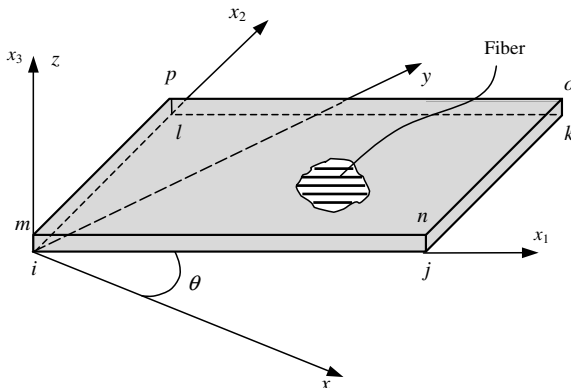


Fig. 1. The cross-ply laminated plate and the coordinate systems.

physical parameters throughout an element are assumed to be the same.

For an eight-node finite element with three degrees of freedom per node, the displacement field over an element is given by

$$\{\delta\} = (u, v, w)^T = \sum_{i=1}^8 [N_i] \{\delta_i\} \quad (1)$$

where  $\{\delta_i\} = (u_i, v_i, w_i)^T$  is the displacement vector at node  $i$ ,  $[N_i] = N_i [I_3]$ ,  $[I_3]$  is a three-order unit matrix and  $N_i$  the shape function [32]. Then the strain vector of each element can be expressed in terms of displacement in the global coordinate system as

$$\{\varepsilon^e\} = (\varepsilon_{11}^e, \varepsilon_{22}^e, \varepsilon_{33}^e, \varepsilon_{12}^e, \varepsilon_{13}^e, \varepsilon_{23}^e)^T = \sum_{i=1}^8 [B_i] \{\delta_i\} \quad (2)$$

where

$$[B_i] = [A][N_i] \quad (3)$$

and

$$[A] = \begin{bmatrix} \frac{\partial}{\partial x} & 0 & 0 \\ 0 & \frac{\partial}{\partial y} & 0 \\ 0 & 0 & \frac{\partial}{\partial z} \\ \frac{\partial}{2\partial y} & \frac{\partial}{2\partial x} & 0 \\ 0 & \frac{\partial}{2\partial z} & \frac{\partial}{2\partial y} \\ \frac{\partial}{2\partial z} & 0 & \frac{\partial}{2\partial x} \end{bmatrix} \quad (4)$$

Thus, the strain vector in an element can be expressed in terms of nodal displacements as

$$\{\varepsilon^e\} = [B] \{\delta^e\} \quad (5)$$

with

$$[B] = [[B_1], [B_2], \dots, [B_8]] \quad \text{and}$$

$$\{\delta^e\} = (\{\delta_1\}^T, \dots, \{\delta_8\}^T)^T$$

Therefore, the stresses of an element in the global coordinate system can be expressed by the nodal displacements as

$$\{\sigma^e\} = (\sigma_{11}^e, \sigma_{22}^e, \sigma_{33}^e, \sigma_{12}^e, \sigma_{13}^e, \sigma_{23}^e)^T = [K^e] \{\delta^e\} \quad (6)$$

where  $[K^e]$  is the element stiffness matrix as

$$[K^e] = \int_{V_e} [B]^T [A][C][A]^{-1} [B] dV \quad (7)$$

where

$$[C] = \begin{bmatrix} \frac{1}{E_1} & \frac{-\nu_{12}}{E_1} & \frac{-\nu_{13}}{E_1} & 0 & 0 & 0 \\ \frac{-\nu_{12}}{E_1} & \frac{1}{E_2} & \frac{-\nu_{23}}{E_2} & 0 & 0 & 0 \\ \frac{-\nu_{13}}{E_1} & \frac{-\nu_{23}}{E_2} & \frac{1}{E_3} & 0 & 0 & 0 \\ 0 & 0 & 0 & \frac{1}{G_{12}} & 0 & 0 \\ 0 & 0 & 0 & 0 & \frac{1}{G_{13}} & 0 \\ 0 & 0 & 0 & 0 & 0 & \frac{1}{G_{23}} \end{bmatrix}^{-1}$$

is the matrix of material constants with  $E_1, E_2, E_3, G_{12}, G_{13}, G_{23}, \nu_{12}, \nu_{13}$  and  $\nu_{23}$  being the orthotropic elastic constants of an individual lamina, and

$$[A] = \begin{bmatrix} \cos^2 \theta & \sin^2 \theta & 0 & 0 & 0 & -2 \sin \theta \cos \theta \\ \sin^2 \theta & \cos^2 \theta & 0 & 0 & 0 & 2 \sin \theta \cos \theta \\ 0 & 0 & 1 & 0 & 0 & 0 \\ 0 & 0 & 0 & \cos \theta & \sin \theta & 0 \\ 0 & 0 & 0 & -\sin \theta & \cos \theta & 0 \\ \sin \theta \cos \theta & -\sin \theta \cos \theta & 0 & 0 & 0 & \cos^2 \theta - \sin^2 \theta \end{bmatrix}$$

is the transform matrix between the local and global coordinate systems.

After assembly of the nodal displacements of all elements, the total strain energy of a multi-layer composite plate can be represented as

$$U = \frac{1}{2} \{\delta\}^T [K] \{\delta\} \tag{8}$$

where  $\{\delta\}$  and  $[K]$  are the global nodal displacement vector and stiffness matrix, respectively. From the eigenvalue problem of

$$([K] - \omega^2 [M]) \{\delta\} = 0 \tag{9}$$

the modal parameters such as natural frequencies  $\omega_i$ , mode shapes, modal strains, etc., can be obtained. In Eq. (9)  $[M]$  is the global mass matrix.

For an arbitrary intact laminated plate, in order to ensure the material continuity, the displacements and their variations of each pair of coincident nodes on the upper and lower adjacent laminae have to be equal in the whole process of computation. When the plate is delaminated, the displacements of each pair of coincident nodes just on the upper and lower surfaces within the delamination region are considered not to be connected to each other.

### 3. Wavelet packet decomposition of vibration signals and its energy spectrum

As a new algorithm for signal processing and data compression, wavelet transform has been used for multi-resolution signal representation since last decade [33–37]. Wavelet packets are the generalization of the compactly supported wavelets as described in [38]. If  $\phi(t)$  is any ‘sufficiently nice’ function with mean 0, by defining its modulation, dilation, and translation as  $e^{if t} \phi(t)$ ,  $s^{1/2} \phi(st)$ , and  $\phi(t - p)$ , respectively, the collection of modulated, dilated and translated  $\phi$ ’s forms a family of wavelet packets with parameters  $f$ ,  $s$  and  $p$ . Energy conservation is satisfied during these transformations, so the waveforms can be normalized as unit vectors. The component of a function  $x$  at  $f$ ,  $s$ ,  $p$  is the inner product of  $x$  with the modulated waveform, whose parameters are  $f$ ,  $s$ , and  $p$ . If it is large, we may conclude that  $x$  has considerable energy near frequency  $f$ , scale  $s$  and position  $p$ . Therefore, wavelet packet decomposi-

tion has an effective application to analysis on vibration response, especially nonsteady signals.

Roughly speaking, a wavelet packet is a square integrable modulated waveform with mean 0. It is well localized in both position and frequency, and can be assigned three parameters, i.e., frequency, scale, and position. If  $\psi$  is a wavelet packet, the frequency and position may be taken as the centers of mass of  $|\psi|^2$  and  $|F(\psi)|^2$  with  $F(\psi)$  being the Fourier transform of  $\psi$ . The scale might be taken as a characteristic width of  $|\psi|^2$ . It is equivalent to the uncertainty in the position and, by Heisenberg’s principle, it is also the reciprocal of the uncertainty of frequency.

#### 3.1. Orthonormal bases and wavelet packets

Generally, an exact quadrature mirror filter  $h(k)$  is defined as

$$\sum_k h(k - 2i)h(k - 2j) = \delta_{i,j}, \quad \sum_k h(k) = \sqrt{2} \tag{10}$$

In multi-resolution analysis, the orthonormal scaling function  $\phi(t)$  and wavelet function  $\psi(t)$  satisfy the dyadic scaling equation:

$$\phi(t) = \sqrt{2} \sum_k h(k) \phi(2t - k) \tag{11}$$

$$\psi(t) = \sqrt{2} \sum_k g(k) \phi(2t - k) \tag{12}$$

where  $g(k) = h(k + 1)(-1)^k$ . Let  $w_0 = \phi(t)$  and  $w_1 = \psi(t)$ , the above dyadic scaling equations can be expressed as the following recursive equations

$$w_{2n}(t) = \sqrt{2} \sum_k h(k) w_n(2t - k) \tag{13}$$

$$w_{2n+1}(t) = \sqrt{2} \sum_k g(k) w_n(2t - k) \tag{14}$$

Then, the functions  $\{w_n(t)\}$  form an orthonormal basis and are called the orthonormal wavelet packets of function  $\phi(t)$ .

#### 3.2. Decomposition of functions in orthonormal wavelet packet bases

If the operations for decomposition of multi-analysis are defined as

$$H[s_k](i) = 2 \sum_k s_k h(k - 2i) \tag{15}$$

$$G[s_k](i) = 2 \sum_k s_k g(k - 2i) \tag{16}$$

Eqs. (13) and (14) can be rewritten as

$$w_{2n}(t - l) = H[w_n(2t - k)](l) \tag{17}$$

$$w_{2n+1}(t - l) = G[w_n(2t - k)](l) \tag{18}$$

Thus, we have

$$w_n(t-l) = \sqrt{2} \sum_k h(l-2k)w_{2n}\left(\frac{t}{2}-k\right) + g(l-2k)w_{2n+1}\left(\frac{t}{2}-k\right) \quad (19)$$

If a signal  $f(t)$  satisfies

$$f(t) = \sum_k s_k^j w_n(2^{-j-1}t-k) \quad (20)$$

its  $j$ -layer binary decomposition in the basis of orthonormal wavelet packets can be deduced as

$$f(t) = \sqrt{2} \sum_i H[s_k^j](i)w_{2n}(2^{-j-1}t-i) + \sqrt{2} \sum_i G[s_k^j](i)w_{2n+1}(2^{-j-1}t-i) \quad (21)$$

Therefore, by wavelet packet decomposition, any signal can be decomposed into two parts, i.e., the project on  $\{w_{2n}(2^{-j-1}t-1)\}$  operated by  $H$  and that on  $\{w_{2n+1}(2^{-j-1}t-1)\}$  operated by  $G$ . Clearly, wavelet packet decomposition of a signal has better localization effect than that of wavelet and is, therefore, used to adaptively choose the corresponding frequency bandwidth according to the characteristics of the detection signal and to enhance the resolution both in frequency and time domains for damage identification of composites.

### 3.3. Energy spectrum of wavelet packets and extraction of damage index

As the differences of signals between intact and damaged structures are generally insignificant in the early stage of damage, extraction of damage index directly from the measured form of signal (even decomposed by wavelet packets) is still difficult. Therefore, the energy spectrum analysis is used to enhance the sensitivity of features to damage.

The second order norm of an original signal  $f(t)$  is

$$\|f\|_2^2 = \int_R |f(x)|^2 dx \quad (22)$$

Then, it is the equivalent energy of the original signal in time domain. For allowable wavelet  $\psi$ , we have

$$\iint_R |W_\psi f(a,b)/a|^2 db da = \|f\|_2^2 \quad (23)$$

Thus, there is an equivalent relationship between the energy of wavelet transform and that of the original signal. Therefore, it is reliable to express energy variation in the original signal by energy spectrum of the response signal decomposed by wavelet packets. Hence, in the energy spectrum of wavelet packets, the sum of square of the decomposed signal is selected as the energy feature within every subspace (frequency span). In sub-

space  $V_{2^j i}$ , i.e., the  $i$ th frequency span of the  $j$ th layer, the result of wavelet packet decomposition is expressed by  $\{S_i(k), k=1, 2, \dots, M\}$ , and its energy is expressed by

$$U_{2^j i} = \sum_{k=1}^M |S_i(k)|^2 \quad (24)$$

where  $M$  is the length of samples in the subspace. If  $\{U_{2^j i}^0\}$  and  $\{U_{2^j i}^d\}$  represent the energy spectrums of the signals measured from intact and damaged samples, respectively, the dimensionless index

$$\eta_i = \frac{|U_{2^j i}^d - U_{2^j i}^0|}{U_{2^j i}^0} \quad (25)$$

can demonstrate the damage-induced energy variation of the signal in subspace  $V_{2^j i}$ .

As the frequency band is equal for each subspace obtained by wavelet packet decomposition of the signal, a series of columns can be plotted for  $\eta_i$  in every frequency span. Let the sum of all the columns be equal to 1 in a particular layer of decomposition, each of the columns can, therefore, represent the percentage of the sum of energy variation in the subspace about the total variation of energy in the considered layer. In this case, the height of each column is

$$\zeta_i = \frac{\eta_i}{\sum_{k=1}^{2^j} \eta_k} \quad (26)$$

## 4. Numerical analysis on energy dissipation

The introduction of damage into a material or structure generally results in increase of damping, which is related to energy dissipation during vibration [39–42]. The dominant energy dissipation in laminated fibrous composites comes from not only the viscoelastic nature of matrix and/or fiber materials but also the interphase damping [43]. Thus local energy dissipation in the damaged region will increase [44]. Analysis on both the local and total changes of energy dissipation due to delamination can demonstrate the relationship between energy dissipation and delamination size.

### 4.1. Samples

Samples for numerical analysis are the same as those used in experiment in this paper. There are altogether five rectangular plates made of multi-layer carbon fiber-reinforced epoxy composites. Every sample plate has an area of  $240 \times 180 \text{ mm}^2$  and consists of 16 layers in orientation of  $[0^\circ/0^\circ/90^\circ/90^\circ/0^\circ/0^\circ/90^\circ/90^\circ]$ . They are fabricated using TC12K33/S-1 prepreg tapes with a thickness of 0.13 mm. One of the plates is intact and named O and the others named A, B, C and D, respectively, are damaged with delamination of different

areas. The delamination is simulated by inserting a polyester film with thickness of 0.015 mm into the plate. Each polyester film is inserted between the fourth and fifth layers counted from the top of the plate when the samples are fabricated. Every delaminated plate has only one rectangular delamination located at the position with the center as shown in Fig. 2. The delamination areas of plates A, B, C and D are  $18 \times 12$ ,  $36 \times 24$ ,  $54 \times 36$  and  $72 \times 48$  mm<sup>2</sup>, respectively. The material constants of the samples for FEM computation are

$E_1 = 125$  GPa,  $E_2 = E_3 = 8.5$  GPa,  $G_{12} = G_{13} = 4.5$  GPa,  $G_{23} = 3.27$  GPa,  $\nu_{12} = \nu_{13} = \nu_{23} = 0.3$  and  $\rho = 2400$  kg m<sup>-3</sup>.

In order to widely investigate the delamination-induced variations of dynamic behaviors of the samples extensively, two types of boundary conditions are adopted, i.e., plate with four edges free and plate with two edges simply supported and other two edges free as shown in Fig. 2.

#### 4.2. Delamination-induced variation of natural frequency

According to Eq. (9), natural frequencies are computed for the first six modes of the plates with different boundary conditions. Tables 1 and 2 list the natural frequencies for the plates with delamination of different areas. It can be seen that with the increase of delamination area, the natural frequency decreases. The delamination-induced change of natural frequency is however very slight and it is particularly impossible to measure in practice. As accessory information for extensive investigation of delamination-induced energy dissipation, the relationship between natural frequency and delamination size is investigated hereafter.

Figs. 3 and 4 show the percentage changes of natural frequencies with delamination areas, where the height of the column represents the absolute value of the percentage change of natural frequency, i.e.,  $\kappa = |\omega_{\text{damaged}} - \omega_{\text{intact}}| / \omega_{\text{intact}}$ . It is obvious that these absolute values increase with the delamination area. It is also seen that the decrease of natural frequency is not the same for different modes. In the free boundary condition, as shown in Fig. 3, the delamination-induced decreases of natural frequencies are relatively large for modes 2, 4 and 5, and we can hardly see any change of natural

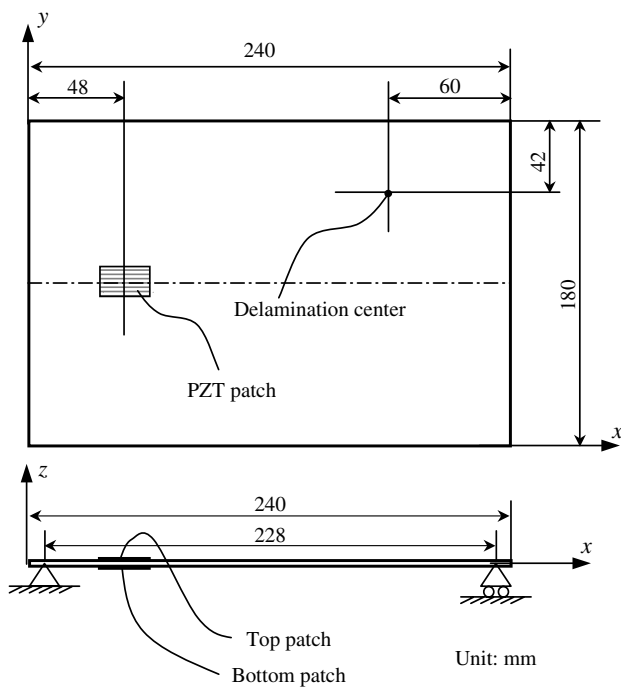


Fig. 2. Sample dimension and the locations of actuators.

Table 1  
Numerical results of natural frequencies for the free plates (Hz)

Mode	Plate O	Plate A	Plate B	Plate C	Plate D
1	90.518	90.518	90.518	90.517	90.515
2	279.17	279.16	279.08	278.66	277.95
3	333.59	333.58	333.52	333.13	332.48
4	354.22	354.21	354.08	353.41	352.06
5	397.62	397.61	397.51	396.96	395.91
6	583.71	583.71	583.68	583.41	582.72

Table 2  
Numerical results of natural frequencies for the simply supported plates (Hz)

Mode	Plate O	Plate A	Plate B	Plate C	Plate D
1	151.95	151.95	151.92	151.75	151.44
2	182.69	182.69	182.67	182.53	182.28
3	450.91	450.9	450.75	449.97	448.45
4	603.98	603.98	603.92	603.18	600.43
5	635.31	635.31	635.25	634.55	632.31
6	844.4	844.37	844.06	842.57	839.64

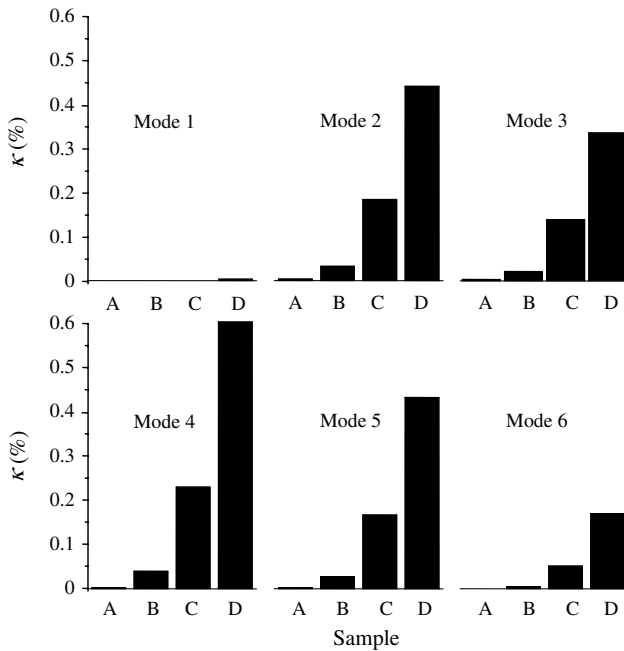


Fig. 3. Percentage changes of natural frequencies for plates with delaminations of different areas in free boundary condition.

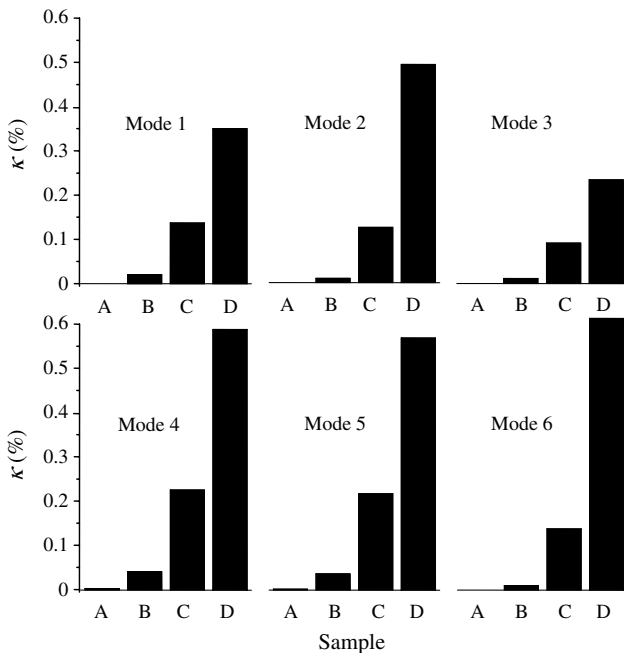


Fig. 4. Percentage changes of natural frequencies for plates with delaminations of different areas in simply supported boundary condition.

frequency in mode 1. The largest change occurs in mode 4 for all the free plates. The relatively large changes of natural frequencies occur in modes 4, 5 and 6 in the case of simply supported condition. However, the variation manner of the values is not the same for each plate. When the delamination area is  $18 \times 12 \text{ mm}^2$ , the delamination-induced changes of natural frequencies are

nearly zero for all the considered cases, which indicates that the delamination-induced frequency change is insignificant for small delamination. Therefore, it is indispensable to analyze the delamination-induced changes of other parameters for effective detection of delamination in composite plates.

### 4.3. Delamination-induced variation of mode shape

The above analysis demonstrates that the delamination-induced changes of plate parameters are mode-dependent. This may imply that the delamination region exerts specific effects on the relevant modes. In order to further investigate the relationship between delamination and mode-dependent variations of energy dissipation in the plate, the unit-normalized local displacements of points within the delamination region of the plates are computed. For the two types of boundary conditions, the relative displacements are analyzed for points along the line ( $y = 138 \text{ mm}$ ,  $z = 1.575 \text{ mm}$ ) just on the upper and lower surfaces within the delamination region of plate B (the plate with delamination area of  $36 \times 24 \text{ mm}^2$ ). Fig. 5 shows, in the case of free boundary condition, the differences of displacement along  $z$ -direction between the upper and lower points ( $\delta w = w_{\text{upper}} - w_{\text{lower}}$ ), which are assumed to be coincident with each other before plate motion. It can be seen that obvious penetrations occur in modes 2 and 4 because of the negative values of  $\delta w$ . As there is no restriction to penetration within the delamination region in the FE model, penetration occurs in some modes. However, this is physically impossible, then, it is known that obvious impact exists within the delamination region in modes 2 and 4 during vibration of the plate. Therefore, energy dissipation variation will be larger in modes 2 and 4 for plate B during vibration. For the same boundary condition, Fig. 6 shows the relative

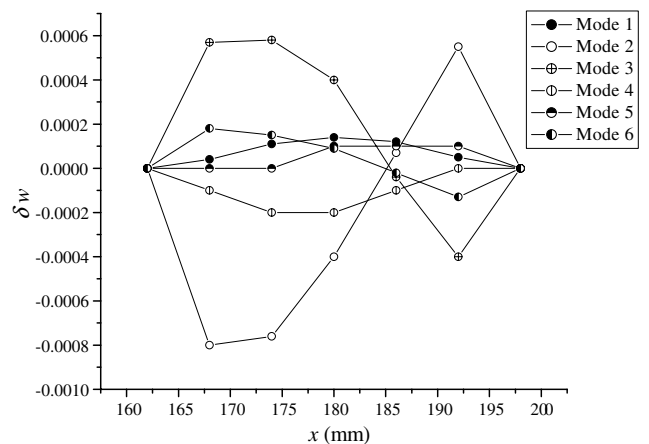


Fig. 5. Displacements along  $z$ -direction for points on the upper and lower surfaces within delaminated region of plate B in free boundary condition.

displacements in  $x$ - $y$  plane for the above mentioned points, where  $d = \sqrt{(u_{upper} - u_{lower})^2 + (v_{upper} - v_{lower})^2}$ . It is seen that the relative displacements are also larger in modes 2 and 4, which implies that, the interactive motion between the upper and lower surfaces within the delamination region is more serious in these two modes than in others for plate B during vibration. Hence, the effect of delamination on the plate is more significant for modes 2 and 4 than in others for plate B in the case of free boundary condition. This result is consistent with that for natural frequency as shown in Fig. 3.

As for the simply supported boundary condition, the differences of displacements between the points just on the upper and lower surfaces within the delaminated region of plate B are also computed and shown in Figs. 7 and 8. Fig. 7 reveals that the physically impossible penetration apparently occurs between the upper and lower surfaces within the delamination region in the fourth mode, which implies that impact occurring in the damaged region is more significant for this mode than for other modes. It is seen from Fig. 8 that the relative in-plane displacements between the coincident points are more serious in modes 4 and 5 than those in other modes for the case of simply supported boundary condition. This means that the interactive motion within the delamination region is severer in modes 4 and 5 than in other modes during the vibration of plate B with simply supported condition. These results are also in accordance with those for natural frequencies as shown in Fig. 4.

Therefore, when delamination occurs somewhere in a composite plate, there may be interactive motion or impact within the delamination region during vibration of the plate. These phenomena cause the variations of energy dissipation in the plate, and they are modal de-

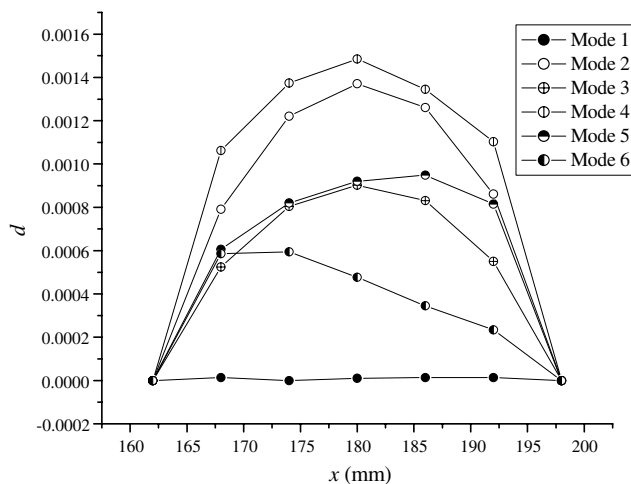


Fig. 6. Relative displacements in  $x$ - $y$  plane for points on the upper and lower surfaces within delaminated region of plate B under free boundary condition.

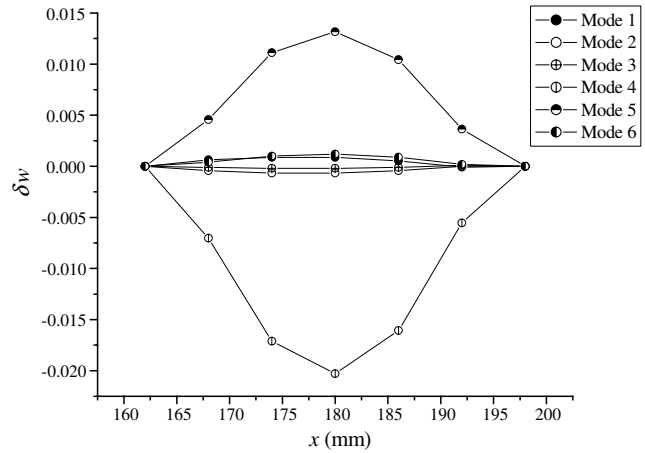


Fig. 7. Displacements along  $z$ -direction for points on the upper and lower surfaces within delaminated region of plate B under simply supported boundary condition.

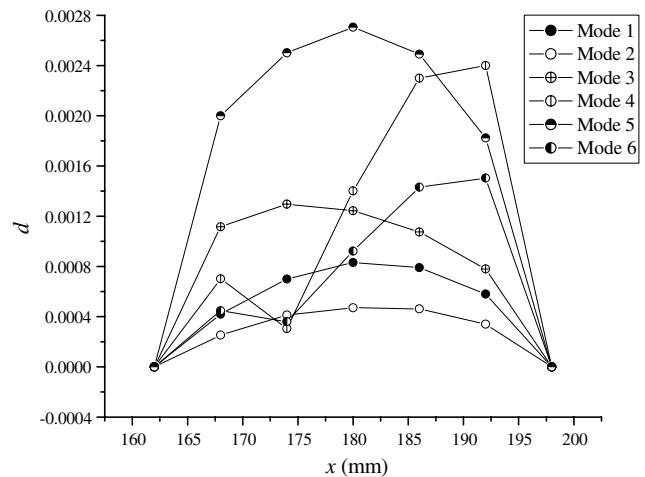


Fig. 8. Relative displacements in  $x$ - $y$  plane for points on the upper and lower surfaces within delaminated region of plate B under simply supported boundary condition.

pendent. Thus, the delamination can be detected according to the variation of energy dissipation in the plate during vibration.

## 5. Vibration signal analysis for delamination determination

### 5.1. Experimental set-up and procedure

Vibration measurements for the above mentioned plates are conducted with the experimental set-up illustrated by Fig. 9. Measurement is performed for the two boundary conditions, respectively, i.e., free and simply

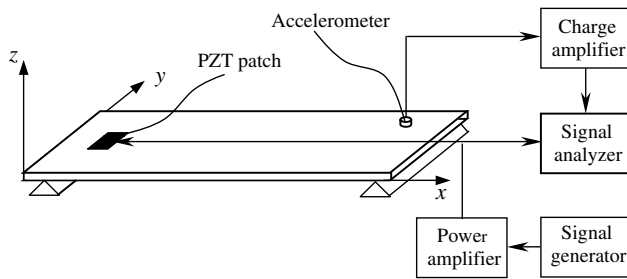


Fig. 9. The experimental set-up for response measurement of the composite plates.

supported conditions. The plate is laid on the sponge foam to simulate the condition of free support.

On the top and bottom surfaces of each plate two piezoelectric patches with thickness of 0.3 mm and area of  $15 \times 25 \text{ mm}^2$  are oppositely bonded as actuators, as shown in Fig. 2. An accelerometer (B&K 4374) is mounted on the top surface. Excitation signals are generated using a waveform generator (TTi TGA1241). A power amplifier (TReK 603) and a charge amplifier (B&K 2635) are used to enhance signals from the generator and transducer, respectively. Both the excitation and response signals are recorded and analyzed by an FFT spectrum analyzer (B&K 3550). The average of eight repeated measurements for each case is taken as the result to reduce the influence of noise.

### 5.2. Wavelet packet decomposition of response signals

Baseline frequency response function (FRF) for every plate is taken firstly using the sinusoidal sweep excitation in a frequency range of 1–1000 Hz. Rectangular windows are used in conjunction with the excitation and

the response. The first six resonant frequencies for all the plates are identified by FRFs as shown in Tables 3 and 4. They show that it is difficult to determine the delaminations according to the measured variations of natural frequencies especially when the damage dimension is relatively small, because in addition to damage, other factors such as fabricating process of samples, support and experimental error can also lead to changes of natural frequencies.

For experimental determination of the delamination according to the variation of energy dissipation in the plate during vibration, acceleration response to random excitation is measured for every plate. The sampling frequency is 2048 Hz, and signals of the first second are recorded. As described in Section 3, the wavelet packet decomposition of the fifth layer is applied to these signals, and then, the percentage of the sum of energy variation in every subspace over the total energy variation in the fifth layer, i.e.,  $\zeta_i$  as expressed in Eq. (26), is obtained as shown in Fig. 10. It can be seen that when the plates are delaminated, there exists variation of energy. As the natural frequencies of the first six modes are between 80 and 600 Hz as shown in Table 3, the frequency range for analysis is limited from 64 to 640 Hz. Thus, within this range the values of  $\zeta_i$ 's in subspaces 9, 12 and 13 are larger than those in other subspaces. It can also be seen that the largest variation of energy occurs in the 12th subspace (named  $W_{12}$ ), in which the frequency range is between 352 and 384 Hz. Fig. 11 shows the decomposition coefficients in  $W_{12}$ . It also shows that with the increase of delamination size, response signals with the above frequencies contribute more and more to the variation of energy dissipation induced by delamination. This result can also be seen in  $W_9$  as shown in Fig. 10. Therefore, the results shown in Figs. 10 and 11 are ac-

Table 3  
Experimental results of natural frequencies of the free plates (Hz)

Mode	Plate O	Plate A	Plate B	Plate C	Plate D
1	90	88	86	87	89
2	289	287	287	277	286
3	318	318	316	319	313
4	354	357	353	353	345
5	386	384	379	381	392
6	570	570	567	560	575

Table 4  
Experimental results of natural frequencies of the simply supported plates (Hz)

Mode	Plate O	Plate A	Plate B	Plate C	Plate D
1	158	156	152	153	154
2	223	217	210	212	215
3	438	436	433	435	427
4	599	596	591	590	550
5	665	658	637	641	642
6	733	734	736	732	728

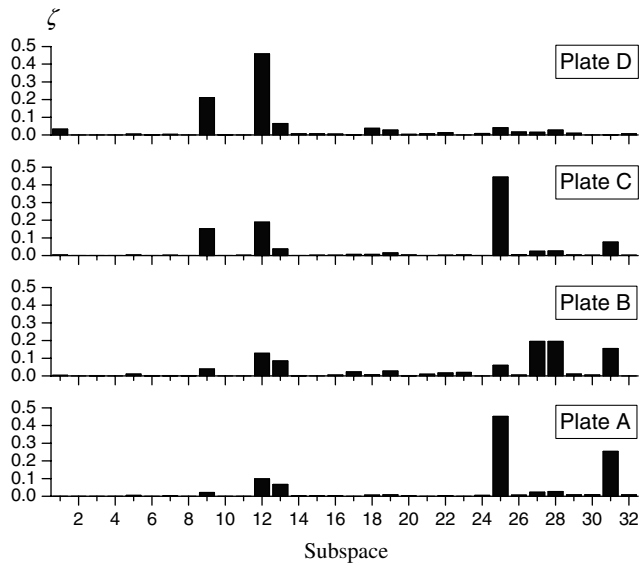


Fig. 10. The percentage of the sum of energy variation of the signal after wavelet packet decomposition for the plates in free boundary condition.

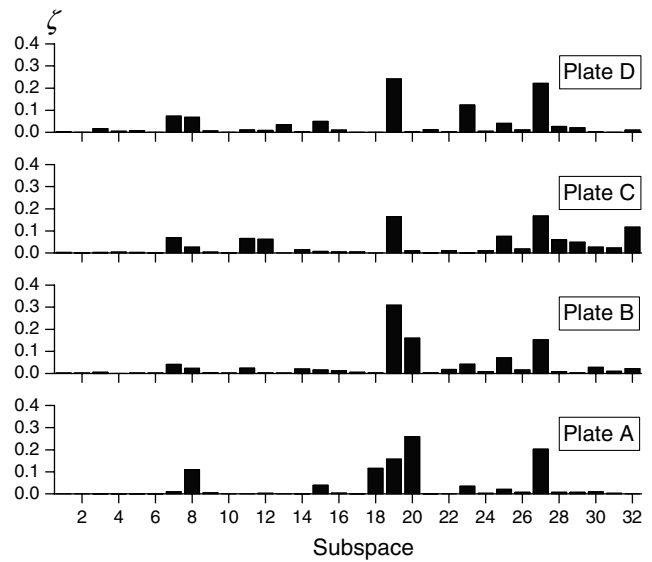


Fig. 12. The percentage of the sum of energy variation of the signal after wavelet packet decomposition for plates in simply supported boundary condition.

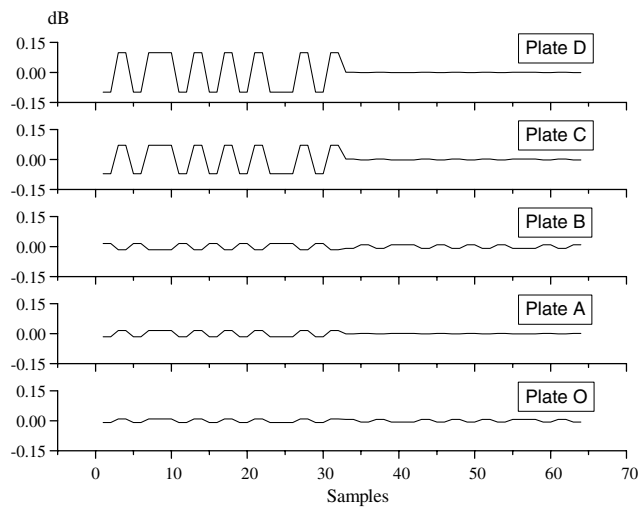


Fig. 11. Wavelet packet decomposition coefficients in subspace 12 for plates in free boundary condition.

cordant with the conclusion yielded in Section 4. However, unlike the natural frequency and mode shape, the energy variation of signals decomposed by wavelet packets is measurable and obvious enough to identify the delamination even for the smallest size considered in this study, i.e. plate A with a delamination area of  $18 \times 12 \text{ mm}^2$ .

As for the simply supported plates, using the response signals to random excitation the wavelet packet decomposition is obtained and the damage index expressed by delamination-induced energy variation is shown in Fig. 12. It is clear that the relatively large energy vari-

ations occur in subspaces 7, 8, 18, 19 and 20 when the analysis frequencies are limited from 128 to 768 Hz. For plate A the variations are very obvious in subspaces 18, 19 and 20. As the frequencies are within 544–640 Hz in these subspaces the results shown by Fig. 12 have a good agreement with that concluded from the numerical analysis as shown in Figs. 3–8. Thus, combined with the numerical analysis as stated in the last section, the delamination-induced energy variation obtained by wavelet packet decomposition can be an effective and practical strategy to identify small delamination.

## 6. Conclusions

Multi-layer composite plates with internal delaminations are analyzed both numerically and experimentally. Using the finite element method, the delamination-induced variation of physical property is studied by analysis of modal parameters, such as natural frequencies and mode shapes. The measured response signal of acceleration to random excitation is processed using wavelet packet decomposition to extract the delamination-induced change of energy dissipation for the vibrating plate. When delamination exists in a composite plate, the natural frequencies and mode shapes are changed, and this change is too slight to be practically determined for small damage. The change of physical property is proved mode-dependent and as the result of energy dissipation variation due to the impact and interactive motion in the delamination region. Even for a delamination smaller than  $18 \times 12 \text{ mm}^2$  in a 16-layer composite plate with a size of  $240 \times 180 \text{ mm}^2$ , the

delamination-induced change of physical property can be practically detected by measurement of response signal to random excitation when the energy spectrum of wavelet packet decomposition is used as the index of damage-induced variation.

### Acknowledgements

The work described in this paper is supported by the Research Grants Council of Hong Kong Special Administrative Region, China (Project No. PolyU 5174/01E). The authors are also grateful for the support of The Hong Kong Polytechnic University to carrying out this project.

### References

- [1] Tasi SW, Hann HT. Introduction to composite materials. Westport, CT: Technic Publishing Company; 1980.
- [2] Voyiadjis GZ. Damage in composite materials. Amsterdam, New York: Elsevier; 1993.
- [3] Gadelrab RM. The effect of delamination on the natural frequencies of a laminated composite beam. *J Sound Vib* 1996;197(3):283–92.
- [4] Osset Y, Roudolff F. Numerical analysis of delamination in multi-layered composite plates. *Comput Mech* 2000;20(1–2):122–6.
- [5] Gerardi TG. Health monitoring aircraft. *J Intell Mater Syst Struct* 1990;1:375–85.
- [6] Mook G, Pohl J, Michel F. Damage detection and characterization in smart CFRP composites. In: Proceedings of SPIE—The International Society for Optical Engineering, San Diego, 18–19 March 2002. p. 120–8.
- [7] Edmonds J, Hickman GA. Damage detection and identification in composite aircraft components. *IEEE Aerospace Conference Proceedings, Big Sky, MT*, 18–25 March 2000. p. 263–70.
- [8] Yam LH, Li YY, Wong WO. Sensitivity studies of parameters for damage detection of plate-like structures using static and dynamic approaches. *Eng Struct, J Earthquake, Wind Ocean Eng* 2002;24:1465–75.
- [9] Castellini P, Revel GM. Laser vibration measurement for damage detection on composite materials. In: Advances in signal processing, Proceedings of SPIE—The International Society for Optical Engineering, Ancona, 21–23 June 2000. p. 442–52.
- [10] Eberle K, Kroeplin B. Vibration measurements and computations for nondestructive testing of damaged composites. In: Proceedings of the International Conference on Computational Methods and Experimental Measurements, Sorrento, 27–29 April 1999. p. 493–502.
- [11] Yan YJ, Yam LH. Online detection of crack damage in composite plates using embedded piezoelectric actuators/sensors and wavelet analysis. *Comput Struct* 2002;58(1):29–38.
- [12] Whelan M. Damage detection in vibrating composite panels using embedded fibre optic sensors and pulsed-DPSI. *Key Eng Mater* 1999;167–168:122–31.
- [13] Doyle C, Fernando G. Detecting impact damage in a composite material with an optical fibre vibration sensor system. *Smart Mater Struct* 1998;7(4):543–9.
- [14] Li YY, Cheng L, Yam LH, Wong WO. Identification of damage locations for plate-like structures using damage sensitive indices: strain modal approach. *Comput Struct* 2002;80(25):1881–94.
- [15] Lichtenwalner PF, Sofge DA. Local area damage detection in composite structures using piezoelectric transducers. In: Proceedings of SPIE—The International Society for Optical Engineering, San Diego, 3–5 March 1998. p. 509–15.
- [16] Tayeb MM. Modal testing to detect and locate damages in large composite structures. In: Proceedings of the International Modal Analysis Conference, Santa Barbara, 2–5 February 1998. p. 334–41.
- [17] Sujatha C, Thanooja S, Rao M, Hanumantha SS. Study on change in modal parameters with damage in composite specimens. In: Proceedings of the International Modal Analysis Conference, Orlando, 3–6 February 1997. p. 1607–13.
- [18] Pidaparti RMV. Free vibration and flutter of damaged composite panels. *Compos Struct* 1997;38(1–4):477–81.
- [19] Viljoen HJ, Van Rensburg NFJ. Damage detection in composites by ZnO sensors. *AICHE J* 1996;42(4):1101–7.
- [20] Cheikh M. Reanalysis of structures with modification of the stiffness, application to the modeling of damage in unidirectional composites. *Comput Struct* 2000;78(5):725–36.
- [21] Mitrovic M, Carman GP, Hickman GA, Bar-Cohen Y. Influence of damage on the vibration response of composite laminates. *Am Soc Mech Eng, Mater Div (Publ) MD* 1995;69-1:371–9.
- [22] Yan YJ, Yam LH. Online detection of crack damage in composite plates using embedded piezoelectric actuators/sensors and wavelet analysis. *Compos Struct* 2002;58(1):29–38.
- [23] Lihua S, Bin C, Shenfang Y, Baoqi T. Experimental research on acousto-ultrasonic inspection of composites by PZT patches and wavelet analysis. In: Proceedings of SPIE—The International Society for Optical Engineering, Newport Beach, 5–6 March 2001. p. 259–66.
- [24] Yam LH, Yan YJ, Jiang JS. Vibration-based damage detection for composite structures using wavelet transform and neural network identification. *Compos Struct* 2003;60(4):403–12.
- [25] Salawu OS. Detection of structural damage through changes in frequency: a review. *Eng Struct* 1997;19:718–23.
- [26] Rytter A, Kirkegaard PH. Vibrational-based inspection of a steel mast. In: Proceedings of the 12th International Modal Analysis Conference, Hawaii, 1994. p. 1602–8.
- [27] Silva JM, Gomes AJM. On the use of modal analysis for fatigue crack detection in simple structural elements. In: Proceedings of the International Offshore Mechanics and Arctic Engineering Symposium, Calgary, Alberta, 7–12 June 1992. p. 595–600.
- [28] Cawley P, Adams RD. The location of defects in structure from measurements of natural frequencies. *J Strain Anal* 1979;4:49–57.
- [29] Sanders D, Kim YI, Stubbs RN. Non-destructive evaluation of damage in composite structures using modal parameters. *Exp Mech* 1992;32:240–51.
- [30] Ceravolo R, Stefano AD. Damage location in structure through a connectivistic use of FEM modal analyses. *Int J Anal Exp Modal Anal* 1995;10(3):178–86.
- [31] Crema LB, Castellani L, Romani A. Damage detection by eigenfrequency measurements in macroelement divided structures. In: Proceedings of the International Modal Analysis Conference, Orlando, 3–6 February 1997. p. 476–83.
- [32] Bathe KJ. Finite element procedures in engineering analysis. Englewood Cliffs, NJ: Prentice-Hall; 1982.
- [33] Mallat SG. A theory for multiresolution signal decomposition: the wavelet representation. *IEEE Trans Pattern Anal Machine Intell* 1989;11(7):674–93.
- [34] Daubechies I. The wavelet transform, time frequency localization and signal analysis. *IEEE Trans Inf Theory* 1990;36(5):961–1005.
- [35] Dapiazl G, Rivola A. Condition monitoring and diagnostics in automatic machines: comparison of vibration analysis technique. *Mech Syst Signal Process* 1997;11(1):53–73.

- [36] Staszewski WJ, Worden K. Classification of faults in gearboxes—pre-processing algorithms and neural networks. *Neural Comput Appl* 1997;5(3):160–83.
- [37] Yang J, Xiang X, Xiong S. Damage detection of roller bearing using wavelet transform. In: *Proceedings of the International Modal Analysis Conference*, Kissimmee, 8–11 February 1999. p. 1980–3.
- [38] Daubechies I. Orthonormal bases of compactly supported wavelets. *Commun Pure Appl Math* 1988;41(7):909–96.
- [39] Smith SW, Zimmerman DC, Bartkowicz TJ, Kim HM. Experiments for damage location in a damped structure. In: *Proceedings of the International Modal Analysis Conference*, Orlando, 3–6 February 1997. p. 1096–102.
- [40] Napolitano KL, Kosmatka JB. Damage detection of highly damped structures using direct frequency response measurements and residual force vectors. In: *Proceedings of SPIE—The International Society for Optical Engineering*, San Diego, 26–27 February 1996. p. 110–21.
- [41] Birman V, Byrd LW. Effect of matrix cracks on damping in unidirectional and cross-ply ceramic matrix composites. *J Compos Mater* 2002;36(15):1859–77.
- [42] Williams C, Salawu OS. Damping as a damage indication parameter. In: *Proceedings of the International Modal Analysis Conference*, Orlando, 3–6 February 1997. p. 1531–6.
- [43] Gibson RF, Hwang SJ, Kwak H. Micromechanical modeling of damping in composites including interphase effects. In: *Proceedings of the 36th International SAMPE Symposium and Exhibition*, San Diego, 15–18 April 1991. p. 592–606.
- [44] Nelson DJ, Hancock JW. Interfacial slip and damping in fiber-reinforced composites. *J Mater Sci* 1978;13:2429–40.